Formation and characterization of shallow junctions in GaAs made by ion implantation and ms-range flash lamp annealing

Duan, J.; Wang, M.; Vines, L.; Böttger, R.; Helm, M.; Zeng, Y. J.; Zhou, S.; Prucnal, S.;

Originally published:

December 2018

Physica Status Solidi (A) 216(2019)8, 1800618

DOI: https://doi.org/10.1002/pssa.201800618

Perma-Link to Publication Repository of HZDR:

https://www.hzdr.de/publications/Publ-28096

Formation and characterization of shallow junctions in GaAs made by ion implantation and ms-range flash lamp annealing

Juanmei Duan*, Mao Wang, Lasse Vines, Roman Böttger, Manfred Helm, Yu-jia Zeng*, Shengqiang Zhou and Slawomir Prucnal

J. Duan, M. Wang, Dr. R. Böttger, Prof. M. Helm, Dr. S. Zhou, Dr. S. Prucnal
Helmholtz-Zentrum Dresden-Rossendorf, Institute of Ion Beam Physics and Materials Research, Bautzner Landstrasse 400, D-01328 Dresden, Germany
juanmei.duan@hzdr.de
J. Duan, Prof. Y. J. Zeng
College of Optoelectronic Engineering, Shenzhen University, Shenzhen 518060, P. R. China
yjzeng@szu.edu.cn
J. Duan, M. Wang
Technische Universität Dresden, D-01062 Dresden, Germany
Dr. L. Vines
Department of Physics/Centre for Materials Science and Nanotechnology, University of Oslo, P.O. Box 1048 Blindern, N-0316 Oslo, Norway

Abstract

With the demand of aggressive scaling in nanoelectronics, further progress can be realized by integration of high mobility semiconductors, such as III-V compound semiconductors, with complementary metal-oxide-semiconductor (CMOS) technology. In this study we present the formation of shallow n-p and p-n junctions in GaAs utilizing ion implantation of S and Zn, respectively, followed by millisecond-range flash lamp annealing (FLA). The distribution of implanted elements obtained by Secondary Ion Mass Spectrometry (SIMS) shows that the FLA process can effectively suppress the diffusion of dopants. Simultaneously, the ms-range annealing is sufficient to recrystallize implanted layer and to activate the dopants. Formation of p-n and n-p junctions is confirmed by current-voltage characteristics. The on/off-current ratio can reach up to 1.7×10^{7} in the n-GaAs:Zn case.

Keywords: GaAs, shallow junction, ion implantation, flash lamp annealing

1. Introduction

III-V compound semiconductors are very attractive for the high-speed and low-power electronics. Due to high electron mobility and low electron effective mass, they can replace silicon in n-type channel for high performance CMOS circuits.[1-4] The electron mobility of bulk intrinsic GaAs can reach up to 8000 $cm^2 V^{-1} s^{-1}$, which is almost sixfold higher than silicon (1450 $cm^2 V^{-1} s^{-1}$), making GaAs the material of choice for the next generation CMOS.[5-7]. The continuous miniaturization of microelectronic devices requires fabrication of ultra-shallow and low resistance junctions.[8-9] The ultra-shallow junction can be realized using ion implantation, monolayer doping,[10-12] plasma doping,[13] surface transfer doping and δ-doping.[14-17] Nowadays, ion implantation is successfully used for the 10 nm node technology.[14] However, the most critical issue is the post-implantation thermal annealing used for the dopants activation and for the reconstruction of the crystal damaged during the implantation process.[5,18,19] On one hand, the annealing temperature must be high enough to activate dopants and to anneal out defects. On the other hand, the thermal budget introduced into the sample must be sufficiently low to suppress the thermal diffusion of dopants in GaAs. In the case of Si based CMOS technology the millisecond range flash lamp annealing (FLA) has been successfully utilized for the fabrication of Fin Field-effect transistors (FinFET) down to 16 nm node.[20]

The ion beam implantation followed by millisecond-range FLA has been successfully utilised to change the optical properties of GaAs by defect modification and band gap engineering via alloying GaAs with nitrogen. Using N implantation and FLA, the band gap of GaAs:N is reduced from 1.45 eV (undoped GaAs) to 1.30 eV for 1% of N.[21] Moreover, proper defect engineering in GaAs leads to a 1.3 μm emission, which is attractive in the field of optical-fibre communications.[22-23] Prucnal *et al*. have also studied the evolution of electronic band structure in (Ga,Mn)As system after FLA.[24] It has been shown that using Mn

implantation followed by FLA up to 0.6% of Mn can be incorporated into the GaAs crystal. The Mn substitutes Ga leading to the formation of p-type paramagnetic (Ga,Mn)As layer.

In this study, we propose the use of strongly non-equilibrium processing to fabricate shallow p-n and n-p junction in GaAs. The recrystallization of S and Zn implanted GaAs layers and dopant activation are realized during millisecond range FLA. It is shown that the junction depth can be well controlled via engineering of the ion implantation energy and annealing parameters (time and temperature). According to the depth distribution of the implanted dopants in GaAs obtained by secondary ion mass spectrometry (SIMS), the ms-range FLA can fully supress the dopant diffusion in GaAs. Simultaneously, the optical and the structural investigations of flash lamp annealed samples suggest that the implanted dopants are fully activated and defects are removed. In addition, the on/off-current ratio of the fabricated p-n junction in Zn doped GaAs can reach up to 1.7×10^{7}. The ideality factor of the diode $\eta=1.3$ extracted from current voltage results.

2. Experiments

The (100) n-type GaAs wafers doped with Te and p-type GaAs doped with Zn were implanted with Zn and S ions, respectively, to form p-n or n-p shallow junctions. Before ion implantation, the required doses/(ion fluences) and the implantation energies which determines the thickness of the doped layer were calculated using stopping range of ions in matter (SRIM) simulation. The average thicknesses implanted layers which corresponds to the n-type and p-type layer formation, respectively, are estimated to be in the in the range of 40 and 65 nm and the project peak concentrations of implanted elements for all samples are in the range of 5×10^{18} cm^{-3}. Zn was implanted with energies of 20 and 40 keV, while S was implanted with energies of 10 and 30 keV. The detailed information about sample preparation is listed in **Table I**. After the ion implantation, GaAs wafers were annealed by FLA for 10 or 20 ms with different annealing energy densities. **Figure 1** shows the scheme of millisecond-

range flash lamp annealing (FLA) tool. It composes of 12 Xe-lamps 25 cm long and reflector to homogenize the flash light deposited on the sample surface and absorbed by annealed wafer. The optical spectrum of the Xe-lamps covers the wavelengths range from 300 up to 800 nm. This means that effectively can annealed samples which absorbs light in the UV-visible spectral range. The flash pulse can be tuned between 0.4 and 20 ms for single pulse. The ultra-short time annealing allows the dedicated annealing of the close to the surface regions while reducing the thermal budget deposited the bulk.[25] The energy density delivered to the GaAs sample surface by flash lamps for 10 and 20 ms was up to 60 and 85 $J \cdot cm^{-2}$, respectively, which corresponds to the maximum peak temperature about 1100 ^{o}C. The temperature at the surface increases with a ramp determined by the rising edge of the flash pulse (about 300 K/ms for the 10 ms pulse length), the cooling rate is in the range of 100 K/ms.

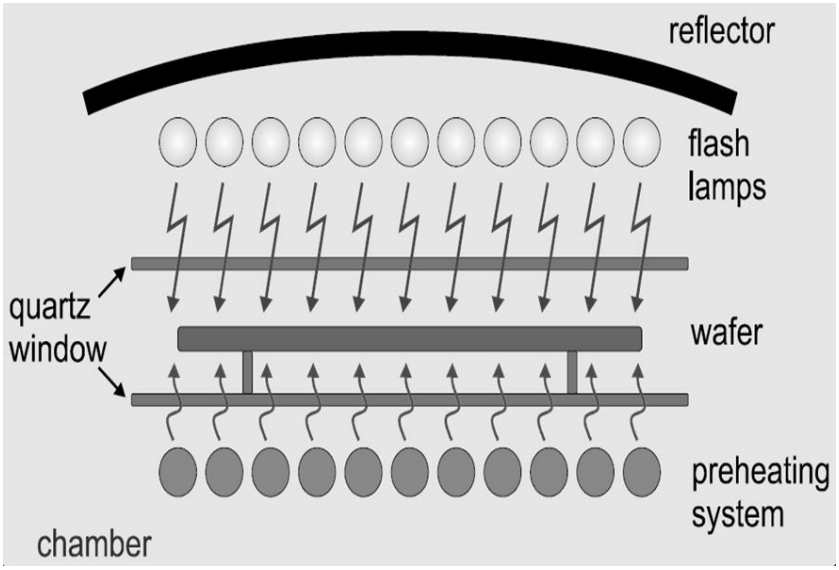

Figure 1. Basics scheme of a FLA tool as used for semiconductor wafer processing.

The optical properties were investigated by photoluminescence (PL) and μ-Raman Spectroscopy. The phonon spectra were measured in a backscattering geometry in the range of 100 to 600 cm^{-1} using a 532 nm Nd:YAG laser with a liquid nitrogen cooled charge coupled device camera. The PL measurements were performed under a blue laser (405 nm) excitation with a maximum excitation power up to 150 mW. The PL spectra were recorded at

the temperature ranging from 10 up to 300 K using a Jobin Yvon Triax 550 monochromator and a cooled InGaAs detector. S concentration versus depth were measured by secondary ion mass spectrometry (SIMS) employing a Cameca IMS7f micro-analyzer to study how the dopants distributions before and after FLA. A beam of 15 keV Cs^+ ions was rastered over a surface area of 200 × 200 μm^2 and secondary ions were collected from the central part of the sputtered crater. Crater depths were measured with a Dektak 8 stylus profilometer, and a constant erosion rate was assumed when converting sputtering time to crater depth. The electrical properties of implanted and annealed samples were investigated using current-voltage (*I-V*) characteristics. The front electrical contacts were made by sputtering Au film through a mask with the circular holes. The Au thickness was 150 nm and the electrical contact diameter was 500 μm. The back side of the sample was fully covered by Au.

TABLE I. Sample preparation: ion energy, fluence, doping range and peak concentrations for shallow junctions.

Samples	Energy (keV)	Fluence (cm^{-2})	Doping range (nm)	Peak concentration (cm^{-3})
n-GaAs:Zn	20	9.5×10^{12}	37	5×10^{18}
	40	1.6×10^{13}	62	5×10^{18}
p-GaAs:S	10	1.0×10^{13}	37	5×10^{18}
	30	2.2×10^{13}	72	5×10^{18}

3. Results and discussion

The influence of the doping and millisecond flash lamp annealing on the microstructural properties of the GaAs was investigated by μ-Raman spectroscopy. The excitation wavelength of Raman laser is 532 nm, corresponding to 7.46×10^4 cm^{-1} of the absorptance coefficient for intrinsic GaAs.[26] Here, we ignore the discrepancy of optical properties between intrinsic GaAs and doped GaAs, so the penetration depth of green laser in GaAs is more than 134 nm.

Therefore the obtained spectra contain signal both from the doped layer and from the substrate. Herein, we only discuss the results obtained from samples implanted with high ion energy (thicker doped layer) to minimize the effect of the substrate on the Raman spectra. Specifically, the GaAs:Zn and GaAs:S referred to the sample implanted with Zn and S with ion energies of 40 keV and 30 keV, respectively. After the ion implantation both samples were annealed for 20 ms with the peak temperature of about 1100 ^{o}C.

Figure 2 shows the μ-Raman spectra recorded from as-implanted and annealed Zn and S doped GaAs samples. The as-implanted GaAs:Zn sample exhibits a noticeable asymmetry on the left side of the longitudinal optical (LO) peak due to overlapping of the Raman signal originating from the substrate and from the implanted layer. Using simple Gaussian deconvolution of the LO phonon mode we found that the main peak located at 292 cm^{-1} is due to the substrate and the much broader and weaker peak at about 285 cm^{-1} coming from the strongly disordered layer formed during ion implantation. The LO peak from annealed GaAs:Zn sample is slightly shifted to lower wavenumbers (291.5 cm^{-1}) compared with that of virgin GaAs (292 cm^{-1}). After FLA, the transverse optical (TO) phonon mode peak at 268.5 cm^{-1} appears. According to the selection rules for the (100) oriented monocrystalline GaAs the TO mode is forbidden but it can be visible in highly-doped p-type GaAs. The shift of the LO phonon mode in Zn doped sample towards smaller wavenumbers is due to the coupling between the plasmon mode and LO mode indicating the incorporation of Zn into the substitutional position and the formation of p-type layer. In annealed GaAs:S cases, the LO phonon mode peak is at 292 cm^{-1}. The LO phonon mode observed from the as-implanted GaAs:S sample is much broader and exhibits a significant asymmetry on the left side of the peak, similar to Zn implanted sample. After FLA, the LO phonon mode is obviously symmetric, indicating a high degree of recrystallization of the implanted layer during the FLA process.

Broadening and decreasing intensity of the LO modes in comparison with virgin GaAs are observed in both annealed GaAs:Zn and GaAs:S samples. This decrease in the intensity and broadening of the LO mode can be related to LO-plasmon coupling.[27-31] The Stokes Raman scattering rate by the LO phonon-damped plasmon mode can be written in the long-wavelength limit by taking into account both the allowed deformation potential and electro-optical contribution as: [29-30]

$$I_s(\omega) = A(n_\omega + 1)\frac{[\omega_{TO}^2(1+C) - \omega^2]^2}{(\omega_{TO}^2 - \omega^2)^2} \times Im[-1/\varepsilon(\omega)] \quad (1)$$

where A is an ω-independent constant factor, n_ω is the Bose-Einstein distribution, C is the Faust-Henry coefficient, ω is the angular frequency, ω_{TO} is the frequency of the TO mode, and $\varepsilon(\omega)$ is the dielectric function given by:

$$\varepsilon(\omega) = \varepsilon_\infty \left[1 + \frac{\omega_{LO}^2 - \omega_{TO}^2}{\omega_{TO}^2 - \omega^2 - i\gamma\omega} - \frac{\omega_P^2}{\omega^2 + i\Gamma_P\omega}\right] \quad (2)$$

Where ε_∞ is the high frequency dielectric constant, ω_{LO} is the frequency of the LO mode, γ is the LO damping factor, and Γ_P is the plasma damping constant. ω_p is the plasma frequency given by:

$$\omega_P^2 = \frac{pe^2}{m_h^* \varepsilon_\infty \varepsilon_0} \quad (3)$$

Where ε_0 is the high frequency dielectric constant, $m_h^*$is the average hole effective mass, and p is the hole concentration. For n-type samples, p is replaced by n (electron concentration) and m_h^* is replaced by the electron effective mass m_e^*. Finally, $I_s(\omega)$ takes the following form: [29-30]

$$I_s(\omega) = \frac{A\omega\Gamma_P\omega_P^2[\omega_{TO}^2(1+C) - \omega^2]^2}{D} \quad (4)$$

with

$$D = [\omega^2(\omega_{LO}^2 - \omega^2) - \omega_P^2(\omega_{TO}^2 - \omega^2) + \gamma\Gamma_P\omega^2]^2 + [\Gamma_P\omega(\omega_{LO}^2 - \omega^2) + \gamma\omega(\omega_P^2 - \omega^2)]^2$$

The mobility μ of the free carriers and their relaxation time τ averaged over all scattering mechanisms, the damping constant Γ_P of the plasma oscillation can be evaluated as follows: [30]

$$\Gamma_P = \tau^{-1} = \frac{e}{\mu m^*} \qquad (5)$$

The line-shape of the LO optical phonon mode is calculated using equation (4). **Table II** presents the values of the fitting parameters obtained from the fitting of the experimental results (see Fig. 2).

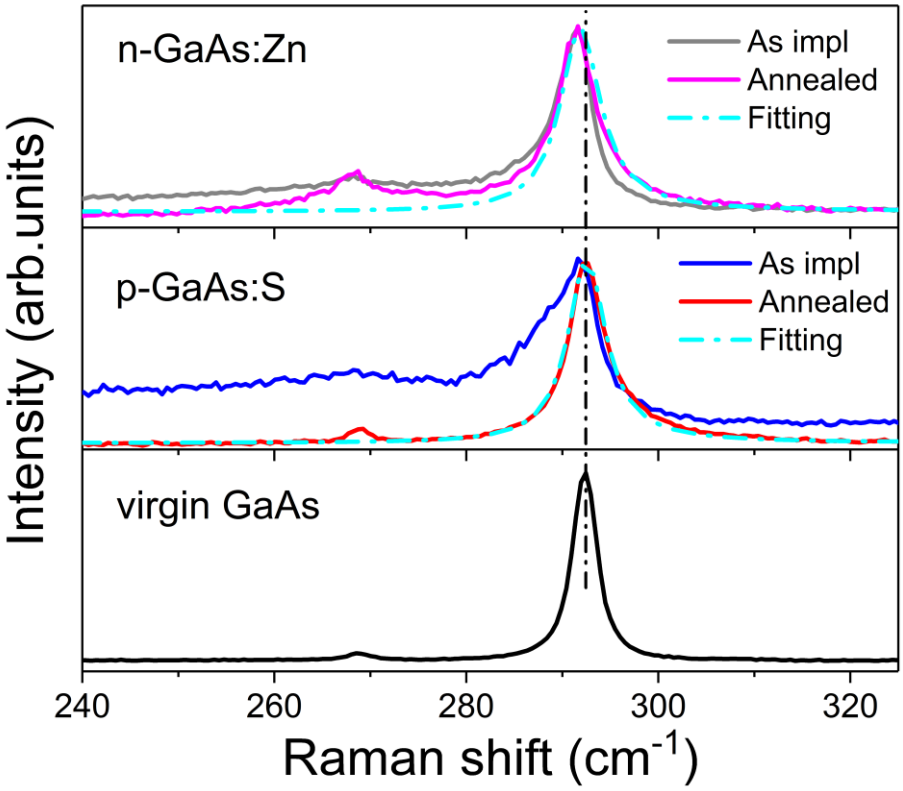

Figure 2. The Raman spectra obtained from annealed and as-implanted Zn and S doped GaAs and virgin GaAs.

We also calculate the carrier concentration and mobility using equation (3) and (5). The carrier concentration and mobility for n-GaAs:Zn sample is 1.65×10^{18} cm^{-3} and 14.6 $cm^2 V^{-1} s^{-1}$, respectively. Since the peak concentration of implanted Zn in GaAs is 5×10^{18} cm^{-3}, obtained carrier concentration suggests that most of Zn dopants in GaAs is electrically

activated. The relatively low carrier mobility is thought to be related with both Coulomb scattering, hole scattering at residual point defects and impurities, and surface recombination. In the GaAs:S case, the carrier concentration and mobility is 1.10×10^{17} cm^{-3} and 267 $cm^2 V^{-1} s^{-1}$, respectively. The carrier concentration for GaAs:S is one order of magnitude lower than that for Zn doped GaAs , which can be caused by the formation of electrically non-active S-S dimers.[18]

TABLE II. Fitting parameters obtained for the LO phonon-damped plasmon structures and fitting results for carrier concentrations and mobilities.

Sample	ω_p (cm^{-1})	Γ_p (cm^{-1})	γ (cm^{-1})	Carrier concentration (cm^{-3})	Mobility ($cm^2 V^{-1} s^{-1}$)
GaAs:Zn	175	1450	2.0	1.65×10^{18}	14.6
GaAs:S	110	515	2.1	1.10×10^{17}	267

Figure 3 (a) shows the room temperature (PL) spectra obtained from virgin GaAs and Zn and S doped GaAs after FLA for 20 ms. The presented PL spectra are normalized for comparison. The PL obtained from the virgin sample without annealing shows the near band gap (NBG) emission at about 875 nm. The peak position for Zn and S doped GaAs is at about 873 and 882 nm, respectively. The full width at half maximum (FWHM) of PL spectra from implanted and annealed GaAs are significantly broader than that observed from the virgin sample. In fact, due to the fact that the penetration depth of the blue laser used for the PL excitation is deeper than the thickness of the doped layer the presented PL spectra compose signal of the substrate and the implanted layer. The NBE emission peak can be fitted with two Gaussian peaks corresponding to the PL emissions from the substrate and from the implanted layer. In the case of Zn doped n-GaAs the PL peak observed from the substrate and implanted layer is located at about 860 nm and the 876 nm, respectively. After S implantation into p-

GaAs and FLA, the PL peak is at 881 and 870 nm which corresponds to the PL emission from the substrate and doped layer, respectively.

Figure 3(b) shows the low temperature PL spectra obtained from virgin GaAs and implanted layers with Zn and S measured at 10 K. The low temperature PL spectra can be divided into two parts: (i) the NBE PL in the wavelength range of 800-880 nm and the defect related PL above 880 nm. The peak position of the NBE is affected by the type of carriers and doping level. Due to the Burstein-Moss effect the n-type layer exhibits a blue shift of the PL peak position while upon p-type doping the NBE PL peak shifts towards lower energies (red shift) .[32-33] The intrinsic and S doped samples show the NBE and PL observed from the radiative recombination between the arsenic vacancies V_{As} level and the valence band (880-1000 nm). The PL spectrum obtained from Zn doped sample exhibits additional strong luminescence located at about 1200 nm. Which has been studied this phenomenon in our previous works.[22-23] The PL peak located at about 1200 nm corresponds to the transitions from conduction band to X center and V_{As} to X center [22]. Note that the luminescence observed at about 1200 nm is optical-active only in intrinsic and n-type GaAs. In p-type GaAs it is totally quenched and this indicates that the PL peak at about 1200 nm observed from n-GaAs:Zn is originating from the n-type GaAs substrate rather than from the Zn implanted layer.

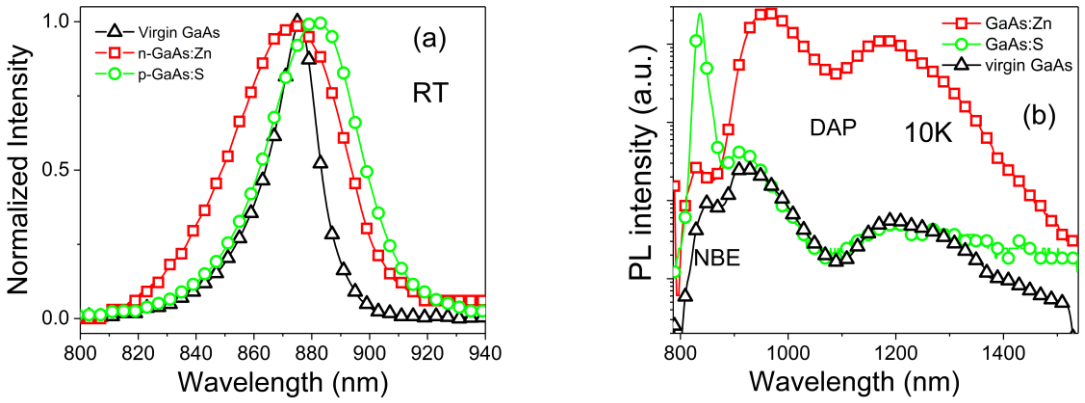

Figure 3. (a) Normalized room temperature photoluminescence spectra obtained from virgin GaAs and ion implanted GaAs after FLA. (b) Low temperature photoluminescence obtained from *n*-GaAs:Zn, *p*-GaAs:S and virgin intrinsic GaAs.

Figure 4 shows the depth distribution of S in GaAs before and after flash lamp annealing for 10 ms at 1100 ^{o}C. S was implanted with energies of 10 keV and 30 keV. Calibration of SIMS system for specific substrate and element is done using as-implanted sample with well know dopant concentration. The depth distribution and concentration of dopants is defined by ion implantation parameters. Apparently, independent of the implantation energy, only very slight diffusion of S is observed, which means that the ms-flash lamp annealing fully suppress the dopant diffusion during high temperature recrystallization process.

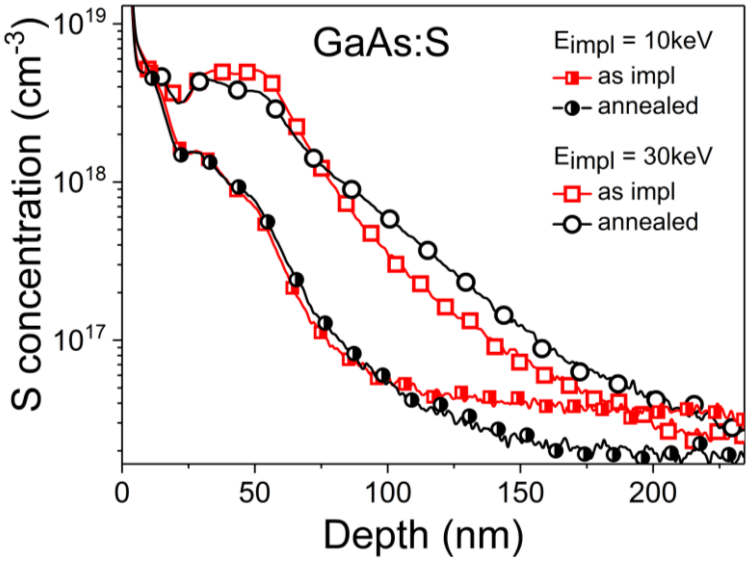

Figure 4. S distribution in as-implanted and annealed p-GaAs:S samples obtained by secondary ion mass spectrometry for implantation energies of 10 and 30 keV.

The distribution of S in GaAs implanted with 10 keV is broader than expected from SRIM simulation. In order to avoid the channeling effect during implantation the ion implantation is performed at the angle of 7 deg between the ion beam and sample surface. The S distribution in GaAs after implantation at 10 keV suggests that at the initial stage of ion implantation a partial channeling took place. Defects introduced into the GaAs during implantation process reduce the channeling and finally the Gaussian distribution of S in GaAs is obtained. The high concentration of S at the surface region (the S concentration higher than 10^{19} cm^{-3}) is due to the measurements instability during the initial stage of sample sputtering (first 10 nm). The

partial channeling can also explain lower concentration of S in GaAs for 10 keV implantation energy than expected from SRIM simulation. Similar diffusion have been reported for Mn implanted GaAs layers annealed by ms-range FLA.[24] Note that the diffusion coefficient of S at 900 ^{o}C in GaAs is in the range of 1×10^{-11} cm^2 s^{-1},[34] and is comparable to the diffusion of Zn in GaAs (1.7×10^{-11} cm^2 s^{-1}).[35] Therefore the influence of the millisecond range FLA on Zn distribution in GaAs should be comparable to S doped sample. In summary the ion implantation followed by ms-range FLA is an effective way for the shallow junction formation in GaAs.

Figure 5 (a) and (b) show the current-voltage characteristics of Zn doped n-GaAs and S doped p-GaAs, respectively. The junction depth was estimated using S and Zn distribution obtained by SRIM simulation in GaAs and is in the range of 40±5 nm. The current-voltage characteristics obtained from processed samples confirm the junction formation and they exhibit the typical diode behavior. Moreover, the on/off-currents are 10^7 and 10^3 for n-GaAs:Zn and p-GaAs:S, respectively, which is the direct evidence that the implanted dopants Zn and S are electrically activated. This also proves our assumption that FLA can be successfully utilized to form a shallow junction in GaAs. The ideality factor extracted from figure 5 (a) is 1.3, which suggests good junction quality and small leakage current. The n-p junction quality made by S implantation and FLA is much worse than that after Zn implantation. This can be attributed to the contact quality and the lack of surface passivation in our test devices. The discrepancy of the quality between p-n and n-p junction is due to the different Fermi-level pinning behavior in p-type and n-type GaAs.[36-37] In the case of p-type GaAs, the Fermi-level position is controlled by intrinsic defects, so the surface Fermi level can move close to the valence band by changing the doping level, especially above 10^{18} cm^{-3}. While in the n-type GaAs, without proper surface passivation the Fermi level is pinned at midgap for all doping levels. Nevertheless the current-voltage characteristics proves that the FLA can be used to activate S in GaAs.

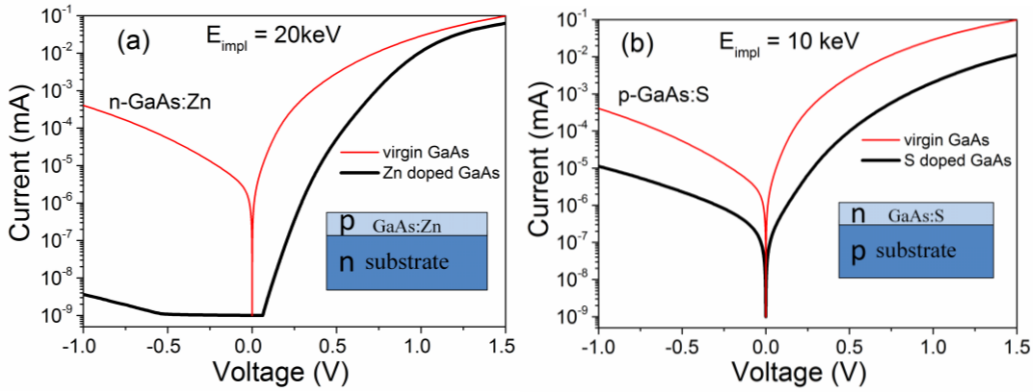

Figure 5. Current-voltage characteristics of implanted and virgin GaAs: the black curves in (a) and (b) shows the I-V curves obtained from n-GaAs:Zn and p-GaAs:S shallow junctions, respectively.

4. Conclusion

In summary, we have fabricated shallow junctions in GaAs by ion implantation of Zn and S into n-type and p-type GaAs, respectively, followed by millisecond range FLA. The carrier concentration estimated from Raman spectra for GaAs:Zn and GaAs:S can reach up to 1.65×10^{18} and 1.1×10^{17} cm^{-3}, respectively. Using FLA the Zn dopants are almost fully activated in GaAs and radiation defects made by ion implantation are removed. According to SIMS data the diffusion of dopants is fully suppressed during ms-range FLA. The on/off-currents ratio and the ideality factor can reach up to 10^7 and 1.3 even without surface passivation in n-GaAs:Zn case. We demonstrate that this single-step FLA processing of ion implanted GaAs prevents the out-diffusion of dopants, which otherwise occur in GaAs during the conventional annealing.

Acknowledgements

Support by the Ion Beam Center (IBC) at HZDR is gratefully acknowledged. The author J. M. Duan acknowledges China Scholarship Council (File No. 201706890037) and Y. J. Zeng acknowledges the National Natural Science Foundation of China (No. 51502178) for financial supports and L. Vines acknowledges the Research Council of Norway through the FriPro projects Salient (Project No. 239895).

References

[1] J. A. Del Alamo, *Nature*. **2011**, *479*, 317.

[2] I. Vurgaftman, J. R. Meyer, L. R. Ram-Mohan, *J. Appl. Phys*. **2001**, *89*, 5815.

[3] K. Tomioka, M. Yoshimura, T. Fukui, *Nature*. **2012**, *488*, 189.

[4] J. Nah, H. Fang, C. Wang, K. Takei, M. H. Lee, E. Plis, *Nano Lett*. **2012**, *12*, 3592.

[5] M. D. McCluskey, E. E. Haller, *Dopants and defects in semiconductors*, CRC Press, Suite, USA, **2012**.

[6] R. Kim, U. E. Avci, I. A. Young, *Proc. IEEE Int. Electron Devices Meeting* (IEDM) **2015,** 15-878, 34.1.

[7] M. Nour, M. Ghoneim, R. Droopad, M. M. Hussain, *Nanotechnology (IEEE-NANO), 2014 14th International Conference on* : IEEE. **2014**, p. 835-8.

[8] J. Barnett, R. Hill, W. Y. Hobbs, C. Hobbs, P. Majhi, R. Jammy, *Junction Technology (IWJT), 2010 International Workshop on* : IEEE. **2010**, p. 1-4.

[9] International technology roadmap for semiconductors (ITRS). 2013 Edition, **2013**.

[10] J. C. Ho, R. Yerushalmi, G. Smith, P. Majhi, J. Bennett, A. Javey, *Nano Lett*. **2009**, *9*, 725.

[11] J. C. Ho, R. Yerushalmi, Z. A. Jacobson, Z. Fan, R. L. Alley, A. Javey, *Nat. Mater*. **2008**, *7*, 62.

[12] L.Ye, M. P. de Jong, T. Kudernac, W. G. van der Wiel, J. Huskens, *Mater. Sci. Semicond. Process*. **2017**, *62* ,128.

[13] Y. S. Kim, H. Kown, *Junction Technology (IWJT), 2017 17th International Workshop on* : IEEE. **2017**, p. 62-5.

[14] C. M. Polley, W. R. Clarke, J. A. Miwa, G. Scappucci, J. W. Wells, D. L. Jaeger, M. Simmons, *ACS Nano*. **2013**, *7*, 5499.

[15] R. E. Camacho-Aguilera, Y. Cai, J. T. Bessette, L. C. Kimerling, J. Michel, *Opt. Mater. Express*. **2012**, *2*, 1462.

[16] W. M. Klesse, G. Scappucci, G. Capellini, M. Y. Simmons, *Nanotechnology* **2011**, *22*, 145604.

[17] W. Chen, D. Qi, X. Gao, A. T. S. Wee, *Progress Surf. Sci.* **2009**, *84*, 279.

[18] E. F. Schubert, *Doping in III-V semiconductors*, USA, **1993**.

[19] S. Zhou, F. Liu, S. Prucnal, K. Gao, M. Khalid, C. Baehtz, M. Helm, *Sci. Rep*. **2015**, *5*, 8329.

[20] P. J. Timans, G. Xing, J. Cibere, S. Hamm, S. McCoy, *Millisecond annealing for semiconductor device applications: Subsecond Annealing of Advanced Materials*, Springer, Switzerland, **2014**.

[21] K. Gao, S. Prucnal, W. Skorupa, M. Helm, S. Zhou, *Appl. Phys. Lett*, **2014**, *105*, 012107.

[22] S. Prucnal, K. Gao, W. Anwand, M. Helm, W. Skorupa, S. Zhou, *Opt. Express*. **2012**, *20*, 26075.

[23] K. Gao, S. Prucnal, W. Skorupa, M. Helm, S. Zhou, *J. Appl. Phys*. **2013**, *114*, 093511.

[24] S. Prucnal, K. Gao, I. Skorupa, L. Rebohle, L. Vines, H. Schmidt, *Phys. Rev. B.* **2015**, *92*, 224407.

[25] S. Prucnal, L. Rebohle, and W. Skorupa. *Materials Science in Semiconductor Processing*, **2017**, *62*, 115.

[26] D. E. Aspnes, A. A. Studna, *Phys. Rev. B.* **1983**, *27*, 985.

[27] K. Wan, J. F. Young, *Phys. Rev. B*. **1990**, *41*, 10772.

[28] J. A. Steele, R. A. Lewis, M. Henini, O. M. Lemine, D. Fan, Y. I. Mazur, *Opt. Express.* **2014**, *22*, 11680.

[29] G. Irmer, M. Wenzel, J. Monecke, *Phys. Rev. B.* **1997**, *56*, 9524.

[30] A. Mlayah, R. Carles, G. Landa, E. Bedel, *J. Appl. Phys*. **1991**, *69*, 4064.

[31] N. I. Goktas, E. M. Fiordaliso, R. R. LaPierre, *Nanotechnology*. **2018**, *29*, 234001.

[32] E. D. Palik, Gallium Arsenide (GaAs), Handbook of optical constants of solids. **1997**.

[33] M. K. Hudait, P. Modak, S. Hardikar, S. B. Krupanidhi, *J. Appl. Phys*. **1997**, *82*, 4931.

[34] J. L. Lee, *J. Appl. Phys*. **1999**, *85*, 807.

[35] H. Bracht, S. Brotzmann, *Phys. Rev. B.* **2005**, *71*, 115216.

[36] M. D. Pashley, K. W. Haberern, R. M. Feenstra, P. D. Kirchner, *Phys. Rev. B.* **1993**, *48*, 4612.

[37] D. Colleoni, G. Miceli, A. Pasquarello. *J. Phys. Condens. Matter*, **2014**, *26*, 492202.